IPP-Report

IPP Max-Planck-Institut für Plasmaphysik

Günter Krainz

Preliminary Studies on Current Leads for WENDELSTEIN 7-X

IPP 11/2

September 1998

Max-Planck-Institut für Plasmaphysik

Preliminary studies on current leads for WENDELSTEIN 7-X

Günter Krainz

Summary

A first study on high-temperature-superconductor (HTSC) current leads for the nuclear fusion experiment WENDELSTEIN 7-X is performed, based on reasonable assumptions concerning design and materials.
The report describes an analytical and a numerical model to calculate the temperature distribution and heat inleak for copper current leads and HTSC current leads at steady state conditions.
Analytical solutions are given for conduction cooled and forced-flow cooled current leads, using the Wiedemann-Franz law.
The numerical model is based on a variational method to solve the two-point boundary value problem in an ordinary differential equation. Nonlinear properties (i.e. specific heat, thermal conductivity) are approximated by polynomial fit functions.
A comparison of results of the analytical and numerical calculation shows good agreement for both, conduction cooled and forced-flow cooled current leads. Small differences in solutions are mainly due to the approximation by the Wiedemann-Franz law. In generall, the analytical method is well suited for parameter studies on different current lead configurations, since the calculating time is much shorter than for the numerical method.

Zusammenfassung

Es wurde eine vorläufige Untersuchung über Hochtemperatursupraleiter-Stromzuführungen für das Kernfusionsexperiment WENDELSTEIN 7-X durchgeführt, die auf realistischen Annahmen bezüglich Design und Materialien basiert.
Der Bericht beschreibt ein analytisches und ein numerisches Modell zur Berechnung der Temperaturverteilung und Wärmeeinleitungsverluste von Kupfer- und Hochtemperatursupraleiter Stromzuführungen bei stationärem Betrieb.
Die analytischen Lösungsansätze beziehen sich auf leitungsgekühlte und zwangsgekühlte Stromzuführungen unter Anwendung des Wiedemann-Franz Gesetzes.
Das numerische Modell basiert auf einer Variationsrechnung zur Lösung des Zwei-Punkt Randwertproblems der gewöhnlichen Differentialgleichung. Nichtlineare Materialeigenschaften (z.B. spezifische Wärme, thermische Leitfähigkeit) werden durch Polynome angenähert.
Der Vergleich von analytischer und numerischer Berechnung zeigt sowohl für leitungs- als auch für zwangsgekühlte Stromzuführungen gute Übereinstimmung. Kleine Abweichungen in den Lösungen sind bedingt durch das Wiedemann-Franz Gesetz. Im allgemeinen eignet sich die analytische Lösung gut für Parameterstudien an unterschiedlichen Stromzuführungskonfigurationen, da die Rechenzeit sehr viel kürzer ist als für die numerische Methode.

Contents

Chapter 1

Introduction

The superconducting magnet system of the W7-X stellarator contains fifty nonplanar main field coils and twenty planar ancillary field coils. The coils form a pentagonally shaped torus of 10 identical segments. Each segment contains five different nonplanar and two planar coil types. Identical coils, distributed regularly over the torus circumference, are connected electrically in series. The design current for powering the superconducting coils is 16 kA. Each group of coils is connected to a separate power supply. Fourteen current leads are needed to power the seven independent main circuits. The current leads generate the majority of heat loss in the cryogenic system [18][19]. The heat leak at the cold end of a current lead is mainly caused by the conducted heat from the hot end at room temperature and from the ohmic loss.
An objective of the current lead design is to minimize the heat leak. A reduction can be attaind by inserting a superconductor shunt at the current lead cold end. This idea is wellknown [2] and led already to considerable success in the development of current leads using low temperature superconductors (LTSC) [4][5]. However, a major improvement could be achieved by using high temperature superconductors (HTSC) not only as shunt for the lower end copper lead but as an independent part of the current lead between the LTSC coil cable and an intermediate temperature level. The advantages of HTSC materials are the high electrical conductivity while acting as thermal insulator at the same time. The height of the intermediate temperature level depends on the proposed cooling concept and on the critical temperature of the superconductor. Experiments on HTSC current leads have been successfully performed for the CERN LHC project up to 13 kA [1][21]. The study shows methods to calculate and optimize the heat inleaks on current leads.

1.1 Overview

This study describes an analytical and numerical model to calculate the temperature distribution along a current lead and the heat inleak at the cold end for steady state conditions.

The *analytical model* is used to optimize the current lead in length and helium mass flow rate with the drawback of loosing accuracy due to approximating the material properties by the Wiedemann-Franz law. It determines the relation between thermal conductivity $\lambda(T)$

and electrical resistivity $\rho(T)$

$$\lambda(T)\,\rho(T) = L_0\,T \tag{1.1}$$

with the Lorentz number $L_0 = 2.445 \cdot 10^{-8}[W\Omega/K^2]$. Most metals obey the Wiedemann-Franz law fairly well [2][23].

The *numerical model* is based on a finite element method without using the Wiedemann-Franz law. Within one segment the temperature dependence of the material properties and the variation of $\Delta T = (T - \theta)$ are neglected. T is the lead temperature and θ is the coolant temperature. Fig. 1.1 shows three reasonable current lead designs [22][24].

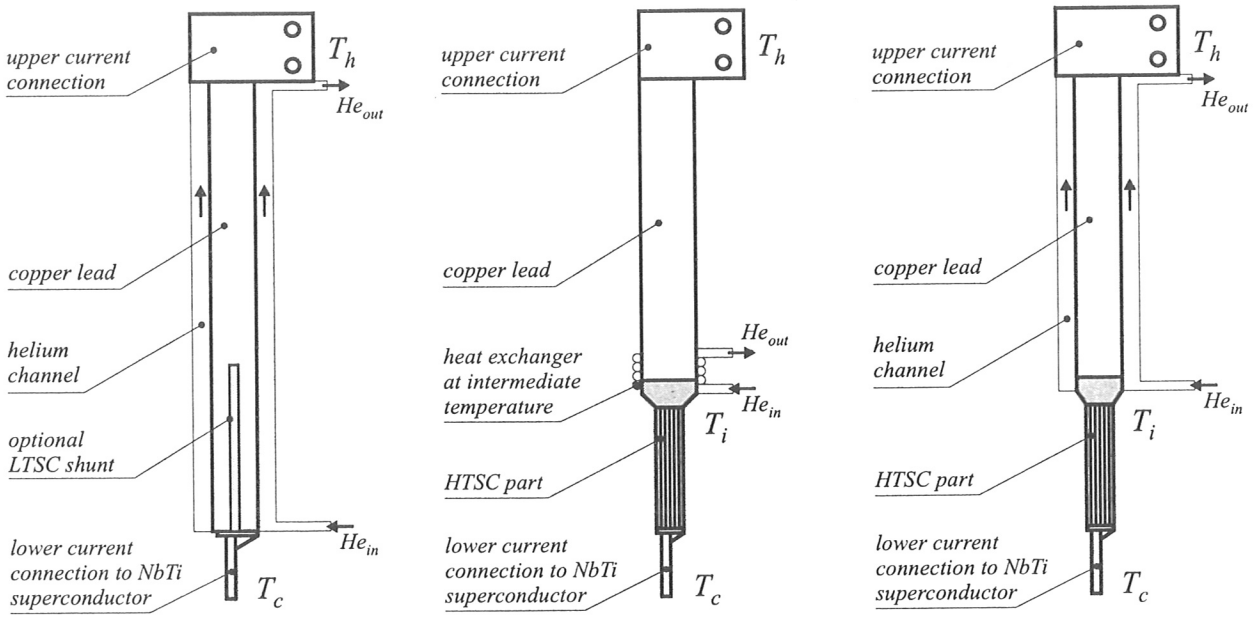

a) Gas cooled copper current lead

b) Combined copper/HTSC current lead with heat exchanger at T_i

c) Gas cooled combined copper/HTSC current lead

Fig. 1.1: Basic current lead configurations

Forced-flow cooled copper current lead: This type of current lead (Fig. 1.1a) will be used as reference model to compare the different current lead designs. Supercritical helium enters the lead at the cold end with temperature T_c and leaves the current lead at the hot end with a temperature of around T_h. The heat leak depends on the current lead geometry l_{cu}/A_{cu}, the electrical current I and the helium mass flow $\dot{m}_{he}$ [17][23]. Equipping the copper conductor with a Nb_3Sn insert at the low temperature part reduces the helium mass flow. As a consequence of the use of superconductor inserts the helium mass flow rate at zero current will be drastically reduced due to the enlarged length of the current lead [8][9].

Combined copper/HTSC current lead with heat exchanger: Fig. 1.1b shows a conduction cooled binary current lead, using a HTSC between the cold end at T_c and an intermediate temperature level at T_i. In order to keep the heat inleak small at the cold end of the lead, the heat exchanger has to absorb the heat at intermediate temperature level. The required helium mass flow in the heat exchanger increases by reducing the temperature difference $(\theta_{out} - \theta_{in})$ [22][24].

Forced-flow cooled combined Cu/HTSC current lead: In configuration Fig. 1.1c, the superconducting section of the current lead is conduction cooled, while the copper section is cooled by gazeous helium. Helium enters at the intermediate temperature level and leaves at room temperature [22].

1.2 Material properties

1.2.1 Electrical resistivity

At low temperatures the electrical resistivity ϱ trends to a constant value, which is strongly dependent on metal purity and amount of lattice imperfections. The value of the residual resistivity ratio

$$RRR = \frac{\varrho(273\ K)}{\varrho(4.2\ K)}$$

is used often as a measure of the purity of the metal. The electrical resistivity of copper is for instance calculated by use of the approximation formula (Unit = $[\Omega m]$)

$$\varrho_{cu}(B, RRR, T) = \left[\frac{1.545}{RRR} + \frac{1}{\frac{2.32547\ 10^9}{T^5} + \frac{9.57137\ 10^5}{T^3} + \frac{1.62735\ 10^2}{T}}\right] 10^{-8} + 0.5\ 10^{-10}\ B \tag{1.2}$$

with an accuracy better than one percent over the temperature range 0 to 1000 K [12][14]. Fig. 1.2 indicates the electrical resistivity of copper as a function of temperature for different values of RRR.

HTSC materials show an unmeasureable low electrical resistance below the critical temperature T_{crit}. It increases rapidly after exceeding T_{crit}. Fig. 1.3 shows a plot for an YBCO superconductor with a critical temperature of 80 K [3].

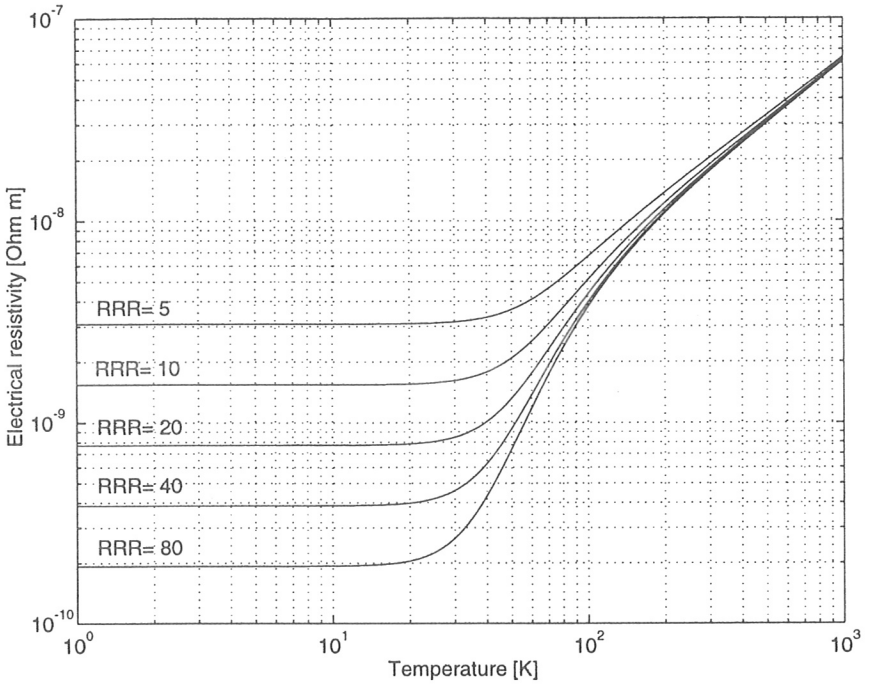

Fig. 1.2: Electrical resistivity of copper versus temperature for different values of RRR

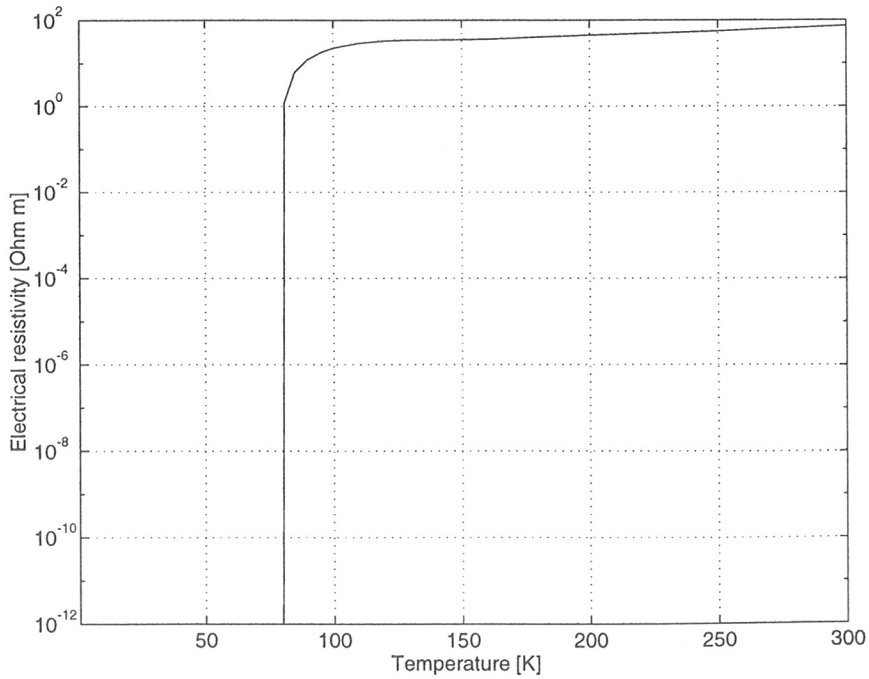

Fig. 1.3: Electrical resistivity of a high temperature superconductor versus temperature

1.2.2 Thermal conductivity

Approximation formulas are given for different temperature ranges [3] (Unit = $[W/(mK)]$):

Copper:

$T \leq 60K$:

$$\lambda_{cu}(B, RRR, T) = \frac{T}{\frac{\varrho(B,RRR,4.2K)}{2.45\ 10^{-8}} + 3.35\ 10^{-7}\, T^3} \left(\frac{2.5}{RRR} + 1\right) \tag{1.3}$$

$60K < T \leq 200K$:

$$\xi = \frac{60}{\frac{\varrho(B,RRR,4.2K)}{2.45\ 10^{-8}} + 3.35\ 10^{-7}\, 60^3} \left(\frac{2.5}{RRR} + 1\right) \left(\frac{3.1}{RRR^2} + \frac{B^2}{100\, RRR} + 1\right)$$

$$\lambda_{cu}(B, RRR, T) = 415 + \frac{-3.36\ 10^{10} + 1,02\ 10^8\, \xi - 6.87\ 10^3\, \xi^2}{T^4} \tag{1.4}$$

$T > 200K$:

$$\lambda_{cu}(B, RRR, T) = 415 \tag{1.5}$$

Fig. 1.4 shows the thermal conductivity of copper. In case of an Ag-Au alloy, sheathed Bi-Pb-Sr-Ca-Cu-O (Bi-2223) superconductor tape, the thermal conductivity of the alloy is about two orders of magnitude higher than that of Bi-2223 (see Fig. 1.5) [6][13][16].
The thermal conductivities of Ag-Au alloy and Bi-2223 [10] are approximated by the following polynomial fit functions (Unit = $[W/(mK)]$):

$Bi_2Sr_2Ca_2Cu_3O_x$ (Bi-2223):

$T \leq 113K$:

$$\lambda(T) = 0.19 + 9.42\ 10^{-3}\, T + 3.4\ 10^{-4}\, T^2 - 6.23\ 10^{-6}\, T^3 + 2.67\ 10^{-8}\, T^4 \tag{1.6}$$

$113K < T \leq 200K$:

$$\lambda(T) = 4.79 - 0.1\, T + 9.9\ 10^{-4}\, T^2 - 4.17\ 10^{-6}\, T^3 + 6.53\ 10^{-9} T^4 \tag{1.7}$$

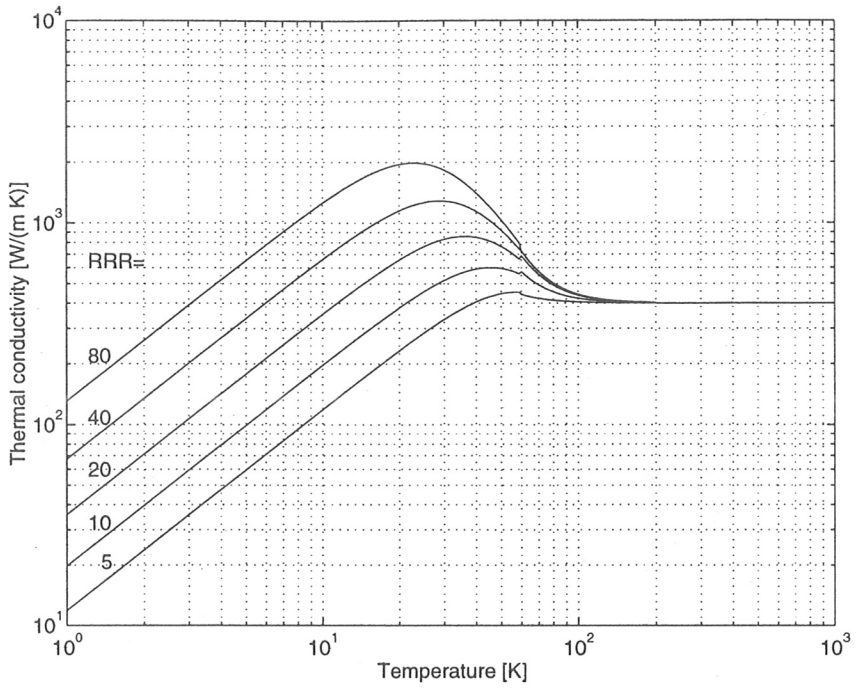

Fig. 1.4: Thermal conductivity of copper versus temperature for different values of RRR

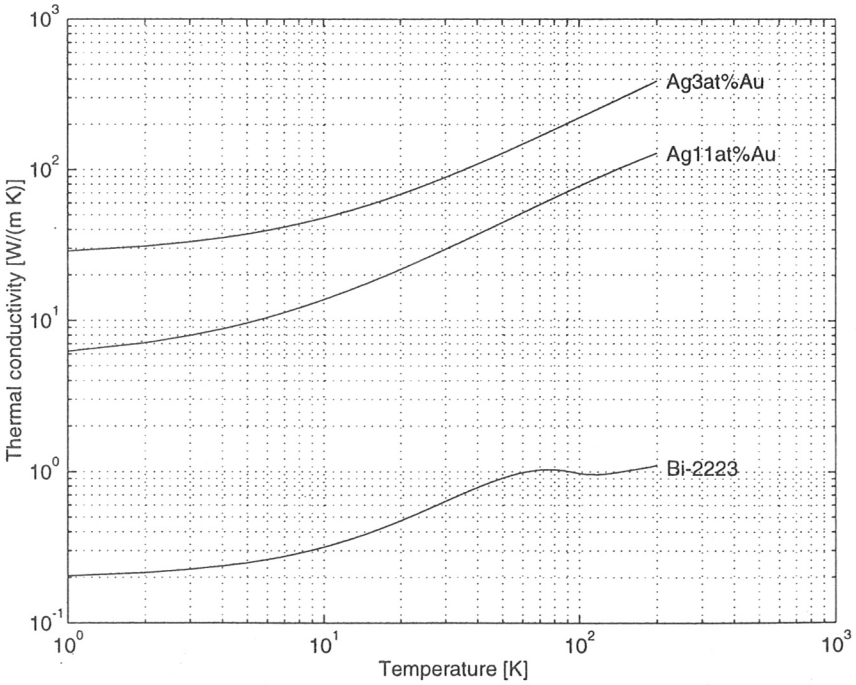

Fig. 1.5: Thermal conductivity of high temperature superconductors versus temperature

Alloy (Ag 3at.%Au):

$T \leq 400K$:

$$\lambda(T) = 26.71 + 2.14\,T - 2.27\ 10^{-3}\,T^2 + 2.99\ 10^{-6}\,T^3 \tag{1.8}$$

Alloy (Ag 11at.%Au):

$T \leq 400K$:

$$\lambda(T) = 5.41 + 8.48\ 10^{-1}\,T - 1.33\ 10^{-3}\,T^2 + 9.03\ 10^{-7}\,T^3 \tag{1.9}$$

1.2.3 Specific heat

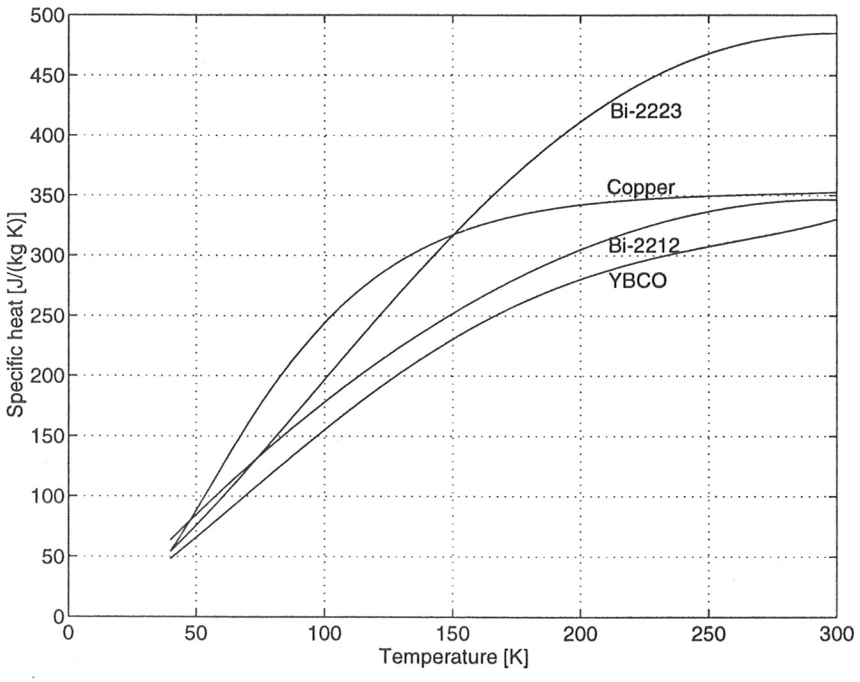

Fig. 1.6: Specific heat of copper and HTSC versus temperature

The specific heat is defined as the heat capacity per unit mass. The heat capacity represents the amount of energy needed to raise the temperature of a material one degree and is a fundamental state property of matter [20].

For modelling, the following approximations have been used (Unit = $[J/(kgK)]$):

Copper (Cu):

$T \leq 20K$:

$$c_p(T) = -2.92\ 10^{-2} + 3.49\ 10^{-2}\,T - 5.44\ 10^{-3}\,T^2 + 1.29\ 10^{-3}T^3 - 2.65\ 10^{-5}\,T^4 + 4.59\ 10^{-7}\,T^5 \tag{1.10}$$

$20K < T \leq 100K$:

$$c_p(T) = 1.92 - 1.04\,T - 6.17\ 10^{-2}\,T^2 + 2.16\ 10^{-4}T^3 - 8.96\ 10^{-6}\,T^4 + 4.09\ 10^{-8}\,T^5 \tag{1.11}$$

$100K < T \leq 300K$:

$$c_p(T) = -306.88 + 10.24\,T - 6.53\ 10^{-2}\,T^2 + 2.13\,10^{-4}T^3 - 3.55\ 10^{-7}\,T^4 + 2.42\ 10^{-10}\,T^5 \tag{1.12}$$

$300K < T \leq 1000K$:

$$c_p(T) = 351.88 + 0.14\,T - 1.24\ 10^{-3}\,T^2 + 3.37\ 10^{-6}T^3 - 2.84\ 10^{-9}\,T^4 + 1.18\ 10^{-12}\,T^5 \tag{1.13}$$

$Bi_2Sr_2Ca_2Cu_3O_x$ (Bi-2223):

$40K < T \leq 300K$:

$$c_p(T) = -11.46 + 1.12\,T - 1.58\ 10^{-2}\,T^2 - 6.91\ 10^{-5}\,T^3 + 7.42\ 10^{-8}\,T^4 \tag{1.14}$$

$Bi_2Sr_2CaCu_2O_x$ (Bi-2212):

$40K < T \leq 300K$:

$$c_p(T) = -28.09 + 2.44\,T - 3.68\ 10^{-3}\,T^2 - 9.68\ 10^{-7}T^3 \tag{1.15}$$

$YBa_2Cu_3O_{7-x}$ (YBCO):

$40K < T \leq 300K$:

$$c_p(T) = -11.48 + 1.18\,T + 1.03\ 10^{-2}\,T^2 - 6.42\ 10^{-5}T^3 + 9.76\ 10^{-8}\,T^4 \tag{1.16}$$

The specific heat of helium c_{phe} is a function of temperature and pressure. Above 10 K and ambient pressure ($\approx 10^5$ Pa) the specific heat is $c_{p_{he}} = 5193$ J/(kg K).

Chapter 2

Analytical model

2.1 Conduction cooled current lead

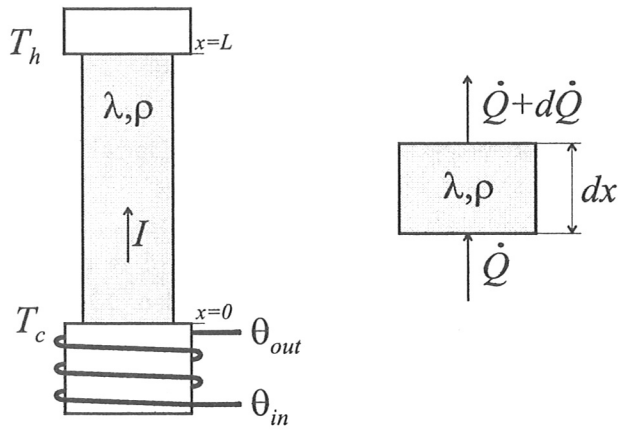

Fig. 2.1: Scheme of a conduction cooled current lead with heat exchanger

Applying the Wiedemann-Franz law (see Eq. (1.1)), the basic differential equation for calculating the one-dimensional temperature distribution along the axis of the conduction cooled current lead (Fig. 2.1) during steady state conditions is [2][17]

$$\frac{d}{dx}\left[\lambda(T)\,A\,\frac{dT}{dx}\right] + I^2\,\frac{\rho(T)}{A} = 0, \tag{2.1}$$

with the cross section area A, the current I, and the temperature T. For an optimized current lead the heat flux at the cold end

$$\dot{Q}_c = \lambda(T)\,A\,\frac{dT}{dx} \qquad \text{at} \qquad x = 0 \tag{2.2}$$

should become a minimum. From Eq. (2.1) follows

$$d\dot{Q} = -\frac{i^2\,\rho(T)}{A}\,dx$$

and further

$$\frac{dT}{dx}\,d\dot{Q} = -\frac{i^2\,\rho(T)}{A}\,dT. \tag{2.3}$$

From this and $\dot{Q} = \lambda(T)\,A\,dT/dx$ follows

$$\dot{Q}\,d\dot{Q} = -\lambda(T)\,\rho(T)\,i^2\,dT. \tag{2.4}$$

The minimum heat flux may be found for constant cross section area across the length. Integration of Eq. (2.4) gives

$$\dot{Q}_c^2 = 2\,i^2 \int_{T_c}^{T_h} \lambda(T)\,\rho(T)\,dT + \dot{Q}_h^2. \tag{2.5}$$

The minimum heat flux $\dot{Q}_c$ at the current lead cold end is obtained when $\dot{Q}_h = 0$ or the temperature gradient dT/dx is zero at the hot end (see also [15]). This leads to the additional boundary condition

$$\frac{dT}{dx} = 0 \qquad \text{at} \qquad x = L.$$

The substitution

$$dz = \frac{dx}{\lambda(T)\,A}$$

and Eq. (1.1) simplify Eq. (2.1) to

$$\frac{d^2T}{dz^2} + I^2\,L_0\,T = 0. \tag{2.6}$$

It has the general solution

$$T(z) = C_1 \sin(\alpha z) + C_2 \cos(\alpha z) \qquad \text{with} \qquad \alpha = I\,\sqrt{L_0}. \tag{2.7}$$

In general, the following boundary conditions are required:

$$\begin{array}{llll} x = 0 & z = 0 & T = T_c & \\ x = L & z = z_h & T = T_h & \frac{dT}{dz} = 0. \end{array}$$

to minimize the heat flux. The cold and hot end temperatures are

$$T_c = C_2$$

$$T_h = C_1 \sin(\alpha z_h) + C_2 \cos(\alpha z_h)$$

with the constants

$$C_1 = \frac{T_h - T_c \cos(\alpha z_h)}{\sin(\alpha z_h)} \qquad \text{and} \qquad C_2 = T_c.$$

The temperature profile as a function of the substituted length z is

$$\boxed{T(z) = T_h \frac{\sin(\alpha z)}{\sin(\alpha z_h)} + T_c \left[\cos(\alpha z) - \frac{\sin(\alpha z)}{\tan(\alpha z_h)}\right]}. \tag{2.8}$$

Hence, the heat leak at the cold end of the current lead becomes

$$\boxed{\dot{Q}_c = \frac{T_h \, \alpha}{\sin(\alpha z_h)} - \frac{T_c \, \alpha}{\tan(\alpha z_h)}}. \tag{2.9}$$

The heat flux changes with z_h and has an optimum at z_h

$$z_{opt} = \left[arctan \frac{\sqrt{T_h^2 - T_c^2}}{T_c} \right] \frac{1}{\alpha}. \tag{2.10}$$

Hence, the length of the current lead section is given by the temperature dependent integral

$$l_{opt} = \int_{z=0}^{z_{opt}} \lambda(T) \, A \, dz. \tag{2.11}$$

2.2 Forced-flow cooled current lead

With use of the Wiedemann-Franz law the basic differential equation for calculating the one-dimensional distribution along the axis of the forced-flow cooled current lead (Fig. 2.2) during steady state conditions is [2]

$$\frac{d}{dx}\left[\lambda(T)\,A\,\frac{dT}{dx}\right] - \beta\,\dot{m}_{he}\,c_{p_{he}}\,\frac{dT}{dx} + I^2\,\frac{\rho(T)}{A} = 0, \tag{2.12}$$

with A the cross section area of the current lead, $c_{p_{he}}$ the specific heat of helium, $\dot{m}_{he}$ the helium mass flow rate, I the current, and T the temperature. The value β defines the efficiency of heat transfer between the current lead and coolant.

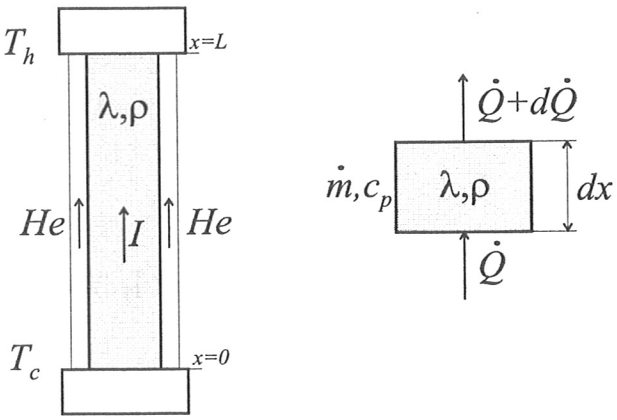

Fig. 2.2: Scheme of a forced-flow cooled current lead

With the substitution

$$dz = \frac{I}{\lambda(T)\,A}\,dx$$

Eq. (2.12) can be written in the form

$$\frac{d^2T}{dz^2} - \frac{\beta\,\dot{m}_{he}\,c_{p_{he}}}{I}\,\frac{dT}{dz} + L_0\,T = 0. \tag{2.13}$$

The characteristic equation of the 2^{nd} order differential equation Eq. (2.13),

$$\xi^2\,T - \frac{\beta\,\dot{m}_{he}\,c_{p_{he}}}{I}\,\xi\,T + L_0\,T = 0$$

has the solutions

$$\xi_{1,2} = \frac{\beta\,\dot{m}_{he}\,c_{p_{he}}}{2\,I} \pm \sqrt{\left(\frac{\beta\,\dot{m}_{he}\,c_{p_{he}}}{2I}\right)^2 - L_0} = \alpha_1 \pm \alpha_2.$$

Dependent on the coefficients in the solution, three different cases have to be considered.

Case 1: $\left(\frac{\beta \dot{m}_{he}\, c_{p_{he}}}{2\,I}\right)^2 > L_0$

The general solution is

$$T(z) = C_1\, e^{(\alpha_1+\alpha_2)z} + C_2\, e^{(\alpha_1-\alpha_2)z} \tag{2.14}$$

with

$$\alpha_1 = \frac{\beta \dot{m}_{he}\, c_{p_{he}}}{2\,I} \qquad \text{and} \qquad \alpha_2 = \sqrt{\alpha_1^2 - L_0}.$$

Boundary conditions for the current lead:

$$\begin{array}{llll} x = 0 & z = 0 & T = T_c \\ x = L & z = z_h & T = T_h \end{array}$$

$$z = \int_0^x \frac{I}{\lambda(T)\,A}\,dx \qquad \text{and} \qquad z_h = \int_0^L \frac{I}{\lambda(T)\,A}\,dx.$$

The cold and hot end temperatures are

$$T_c = C_1 + C_2$$

$$T_h = C_1\, e^{(\alpha_1+\alpha_2)z_h} + C_2\, e^{(\alpha_1-\alpha_2)z_h}.$$

For C_1 and C_2 follows

$$C_1 = -\frac{T_h - T_c\, e^{(\alpha_1-\alpha_2)z_h}}{e^{(\alpha_1-\alpha_2)z_h} - e^{(\alpha_1+\alpha_2)z_h}} \qquad \text{and} \qquad C_2 = \frac{T_h - T_c\, e^{(\alpha_1+\alpha_2)z_h}}{e^{(\alpha_1-\alpha_2)z_h} - e^{(\alpha_1+\alpha_2)z_h}}.$$

The temperature profile along the substituted length z is

$$\boxed{T(z) = T_h\,\frac{e^{(\alpha_1-\alpha_2)z} - e^{(\alpha_1+\alpha_2)z}}{e^{(\alpha_1-\alpha_2)z_h} - e^{(\alpha_1+\alpha_2)z_h}} + T_c\,\frac{e^{(\alpha_1-\alpha_2)z_h}\,e^{(\alpha_1+\alpha_2)z} - e^{(\alpha_1+\alpha_2)z_h}\,e^{(\alpha_1-\alpha_2)z}}{e^{(\alpha_1-\alpha_2)z_h} - e^{(\alpha_1+\alpha_2)z_h}}}. \tag{2.15}$$

The heat leak at the cold end of the current lead becomes

$$\dot{Q}_c = \dot{Q}(z=0) = I\,\frac{dT}{dz}$$

$$\boxed{\dot{Q}_c = I\left[\frac{-2\,T_h\,\alpha_2 + T_c\left[(\alpha_1+\alpha_2)\,e^{(\alpha_1-\alpha_2)z_h} - (\alpha_1-\alpha_2)\,e^{(\alpha_1+\alpha_2)z_h}\right]}{e^{(\alpha_1-\alpha_2)z_h} - e^{(\alpha_1+\alpha_2)z_h}}\right]}. \tag{2.16}$$

Case 2: $\left(\frac{\beta\,\dot{m}_{he}\,c_{p_{he}}}{2\,I}\right)^2 = L_0$

The general solution is

$$T(z) = (C_1 z + C_2)\,e^{\alpha z} \tag{2.17}$$

with

$$\alpha = \frac{\beta \dot{m}_{he} c_{p_{he}}}{2I}.$$

Boundary conditions for an optimized current lead:

$$\begin{array}{llll} x=0 & z=0 & T=T_c \\ x=L & z=z_h & T=T_h. \end{array}$$

The cold and hot end temperatures are

$$T_c = C_2$$

$$T_h = (C_1 z_h + C_2)\,e^{\alpha z_h}$$

with

$$C_1 = \frac{T_h - T_c\,e^{\alpha z_h}}{z_h\,e^{\alpha z_h}} \qquad \text{and} \qquad C_2 = T_c.$$

The temperature profile along the substituted length z is

$$\boxed{T(z) = T_h \frac{z e^{\alpha z}}{z_h e^{\alpha z_h}} + T_c \left(1 - \frac{z}{z_h}\right) e^{\alpha z}}. \tag{2.18}$$

The heat flux at the cold end of the current lead becomes

$$\boxed{\dot{Q}_c = I \left[\frac{T_h}{z_h e^{\alpha z_h}} + T_c \left(\alpha - \frac{1}{z_h}\right)\right]}. \tag{2.19}$$

Case 3: $\left(\frac{\beta \dot{m}_{he}\, c_{p_{he}}}{2I}\right)^2 < L_0$

In this case the general solution is

$$T(z) = [C_1 \sin(\alpha_2 z) + C_2 \cos(\alpha_2 z)]\, e^{\alpha_1 z} \tag{2.20}$$

with

$$\alpha_1 = \frac{\beta \dot{m}_{he}\, c_{p_{he}}}{2I} \qquad \text{and} \qquad \alpha_2 = \sqrt{L_0 - \alpha_1^2}.$$

Boundary conditions for the optimized current lead:

$$\begin{array}{llll} x = 0 & z = 0 & T = T_c \\ x = L & z = z_h & T = T_h. \end{array}$$

The cold and hot end temperatures are

$$T_c = C_2$$

$$T_h = [C_1 \sin(\alpha_2 z_h) + C_2 \cos(\alpha_2 z_h)]\, e^{\alpha_1 z_h}.$$

C_1 and C_2 become

$$C_1 = \frac{T_h - T_c \cos(\alpha_2 z_h) e^{\alpha_1 z_h}}{\sin(\alpha_2 z_h) e^{\alpha_1 z_h}} \qquad \text{and} \qquad C_2 = T_c.$$

The temperature profile along the substituted length z is

$$\boxed{T(z) = T_h \frac{\sin(\alpha_2 z) e^{\alpha_1 z}}{\sin(\alpha_2 z_h) e^{\alpha_1 z_h}} + T_c \left[\cos(\alpha_2 z) - \frac{\sin(\alpha_2 z)}{\tan(\alpha_2 z_h)}\right] e^{\alpha_1 z}}. \tag{2.21}$$

The heat leak at the cold end of the current lead becomes

$$\boxed{\dot{Q}_c = I \left[\frac{T_h \, \alpha_2}{\sin(\alpha_2 z_h) e^{\alpha_1 z_h}} + T_c \left(\alpha_1 - \frac{\alpha_2}{\tan(\alpha_2 z_h)}\right)\right]}. \tag{2.22}$$

Cases 1 and 2 consider the current lead operation at reduced electrical current I and mass flow-rate $\dot{m}_{he}$.

The heat flux $\dot{Q}_c$ has a minimum at $z_h = z_{opt}$ and is determined by numerical optimization. The real length of the lead is given by the result of the integral

$$l_{opt} = I \int_{z=0}^{z_{opt}} \lambda(T) \, A \, dz. \tag{2.23}$$

Operation without current:

In case of zero current the differential equation Eq. (2.12) is written in the form

$$\frac{d}{dx}\left[\lambda(T) \, A \frac{dT}{dx}\right] - \beta \, \dot{m}_{he} \, c_{p_{he}} \frac{dT}{dx} = 0. \tag{2.24}$$

By use of the non-linear substitution

$$dz = \frac{1}{\lambda(T) \, A} \, dx$$

Eq. (2.24) becomes

$$\frac{d^2T}{dz^2} - \beta \, \dot{m}_{he} \, c_{p_{he}} \frac{dT}{dz} = 0. \tag{2.25}$$

With $\alpha = \beta \, \dot{m}_{he} \, c_{p_{he}}$, the common solution is

$$T(z) = C_1 + C_2 \, e^{\alpha z}.$$

Boundary conditions:

$$\begin{array}{llll} x = 0 & z = 0 & T = T_c \\ x = L & z = z_h & T = T_h. \end{array}$$

$$z = \int_0^x \frac{dx}{\lambda(T)\,A} \qquad \text{and} \qquad z_h = \int_0^L \frac{dx}{\lambda(T)\,A}.$$

The temperatures at the cold and hot end of the current lead are

$$T_c = C_1 + C_2$$

$$T_h = C_1 + C_2\, e^{\alpha z_h}.$$

Calculated from the equations above, the constants become

$$C_1 = T_c - \frac{T_h - T_c}{e^{\alpha z_h} - 1} \qquad \text{and} \qquad C_2 = \frac{T_h - T_c}{e^{\alpha z_h} - 1}.$$

The temperature profile as a function of the substituted length z is

$$\boxed{T(z) = T_h \frac{e^{\alpha z} - 1}{e^{\alpha z} - 1} + T_c \left(1 - \frac{e^{\alpha z} - 1}{e^{\alpha z_h} - 1}\right)}. \tag{2.26}$$

The heat leak at the cold end of the current lead becomes

$$\boxed{\dot{Q}_c = (T_h - T_c)\,\frac{\alpha}{e^{\alpha z_h} - 1}}. \tag{2.27}$$

Chapter 3

Numerical model

3.1 Boundary value problem

The numerical design of the current lead is based on a slab, fixed at the temperatures T_c and T_h at the cold end and hot end respectively. This fact leads to a variational method to solve the "boundary value problem" in the ordinary differential equation [11]

$$\frac{d}{dx}\left[\lambda(T)\,A\,\frac{dT}{dx}\right] - h\,p\,(T-\theta) + \frac{\rho(T)\,I^2}{A} = 0 \tag{3.1}$$

with λ the thermal conductivity, ρ the electrical resistivity, A the cross section area, p the wetted perimeter, h the heat transfer coefficient, T the slab temperature, and θ the helium gas temperature. Eq. (3.1) has the boundary conditions

$$T(0) = T_c \text{ and } T(l) = T_h. \tag{3.2}$$

Such a numerically sensitive two-point boundary value problem can be solved by applying a finite difference method. The finite difference equation must incorporate both specific initial and terminal conditions in the finite set of equations. Thus, the resulting solution of these equations is constrained to satisfy these boundary conditions.

3.2 Segmentation of the slab

The slab interval $[0, l]$ is discretized with $N+1$ nodes and N elements, as shown in Fig. 3.1. Ohmic loss generates joule heat Q_r inside the element. Heat Q_λ is conducted along the axis of the slab. In case of gas cooling, Q_{tr} is the part of heat which is absorbed by the surrounding gas.

The second derivative at x_i may be approximated by

$$\frac{d^2T}{dx^2} \approx \frac{T_{j-1} - 2\,T_j + T_{j+1}}{(x_{j+1} - x_j)^2}. \tag{3.3}$$

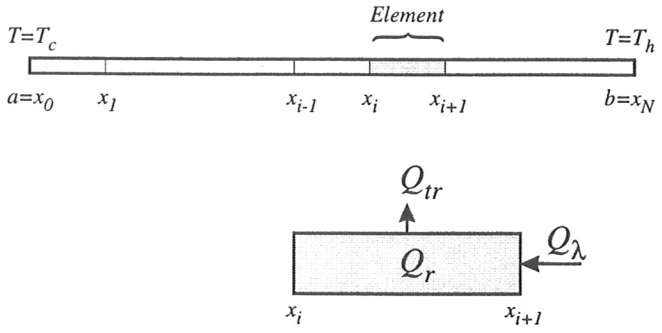

Fig. 3.1: Segmentation of the current lead

Applied to Eq. (3.1) gives for a single element

$$-T_{j-1} + \left(2 + \frac{h\,p}{\lambda\,A}(\Delta x)^2\right) T_j - T_{j+1} = \frac{h\,p\,\theta + j^2\,\rho/A}{\lambda\,A}(\Delta x)^2, \qquad j = 1, 2, \ldots, N. \tag{3.4}$$

The two-point boundary value problem, given by Eq. (3.1) and the boundary conditions in Eq. (3.2) may be approximated by N equations of Eq. (3.4), where the boundary conditions are included. In matrix form the equations appear as

$$\begin{bmatrix} 2+\frac{h\,p}{\lambda\,A}(\Delta x)^2 & -1 & & & 0 \\ -1 & 2+\frac{h\,p}{\lambda\,A}(\Delta x)^2 & -1 & & \\ & \ddots & \ddots & & \\ & & & -1 & \\ 0 & & & -1 & 2+\frac{h\,p}{\lambda\,A}(\Delta x)^2 \end{bmatrix} \begin{bmatrix} T_1 \\ T_2 \\ \vdots \\ T_{N-2} \\ T_{N-1} \end{bmatrix} = \begin{bmatrix} \frac{h\,p\,\theta+i^2\,\rho/A}{\lambda\,A}(\Delta x)^2 & +T_c \\ \frac{h\,p\,\theta+i^2\,\rho/A}{\lambda\,A}(\Delta x)^2 & \\ \vdots & \\ \frac{h\,p\,\theta+i^2\,\rho/A}{\lambda\,A}(\Delta x)^2 & \\ \frac{h\,p\,\theta+i^2\,\rho/A}{\lambda\,A}(\Delta x)^2 & +T_h \end{bmatrix}. \tag{3.5}$$

This is a set of N linear algebraic equations with the N unknowns $T_1, T_2, \ldots, T_{N-1}, T_N$, whose solution is an approximation to the solution Eq. (3.1) at the points x_j.
In matrix expression, Eq. (3.5) is written as

$$\mathbf{A} \cdot \mathbf{T} = \mathbf{b} \tag{3.6}$$

where $\mathbf{A}$ and $\mathbf{b}$ are $N \times N$ and $N \times 1$ matrices respectively. $\mathbf{A}$ is a matrix of three-diagonal character. The temperature in each element is

$$\mathbf{T} = \mathbf{A}^{-1} \cdot \mathbf{b}. \tag{3.7}$$

Steps for calculating the temperature profile:

- Before solving Eq. (3.7), the temperature distribution along the current lead is assumed as a linear function of temperature in order to estimate the non-linear material properties.

- Determining the temperatures according to Eq. (3.7) and updating the material properties. This step will be repeated until the difference between the previous and the new calculated temperature value is less than a specified margin ϵ (i.e. $\epsilon \leq 0.1$ K).
- The heat flux at $T = T_c$ in Fig. 3.1 is approximated with

$$\dot{Q}_c = \lambda(T_c)\, A \frac{T_2 - T_1}{x_2 - x_1}. \tag{3.8}$$

3.3 Coolant Temperature

The temperature of the coolant is calculated from the energy balance

$$\dot{m}\, c_p\, d\theta = h\, p(T - \theta)\, dx \tag{3.9}$$

with c_p the specific heat of the coolant, $\dot{m}$ the coolant mass flow rate, p the wetted perimeter, and h the heat transfer coefficient.
In finite element modelling, the change in coolant temperature over an element is

$$\Delta\theta_j = \frac{h\, p\, (T_j - \theta_j)}{c_p\, \dot{m}} \Delta x. \tag{3.10}$$

Then, the coolant temperature is

$$\theta_j = \theta_{j-1} + \Delta\theta_j. \tag{3.11}$$

Chapter 4

Results from modelling

4.1 Conduction cooled current leads

Calculations have been performed for a single conduction cooled binary current lead (Fig. 1.1b) by varying the intercept temperature level. The intercept temperature

$$T_i = \frac{\theta_{out} - \theta_{in}}{\ln \frac{\theta_{out}}{\theta_{in}}}. \tag{4.1}$$

depends on the inlet and outlet temperature of the cooling gas. The mass flow rate, required to absorb the heat loss at intercept level is

$$\dot{m} = \frac{\dot{Q}_i}{h_{out} - h_{in}} \tag{4.2}$$

with $\dot{Q}_i$ the heat loss at intercept temperature, h_{in} and h_{out} the coolant enthalpy at the heat exchanger inlet and outlet, respectively. The equivalent value of the heat leak at T_c is

$$\dot{Q}_{i_c} = \dot{Q}_i \frac{T_h - T_i}{T_i} \frac{T_c}{T_h - T_c}. \tag{4.3}$$

with $T_c = 4.5$ K and $T_h = 300$ K. The hot end of the HTSC is assumed to have the temperature θ_{out}. Hence, the critical current has to be determined for θ_{out}.
Table 4.1 contains the required mass flow for the heat exchanger and the heat leaks at intercept temperature and at cold end. For calculating the current leads a $RRR = 30$ for the copper section and a current density of $J_{cu} = 10^7$ A/m^2 at 16 kA was assumed, so

$$A_{cu} = \frac{I}{J_{cu}} = \frac{16 \cdot 10^3}{10^7} = 1.6 \cdot 10^{-3} m^2.$$

The length of the copper section is optimized at nominal current with the Neumann condition $dT/dx = 0$ at the hot end. The calculations on conduction cooled current leads assume a

Table 4.1: Results for a single conduction cooled binary current lead

	Units	case 1	case 2	case 3	case 4	case 5	case 6
θ_{in}	[K]	10	20	30	40	50	60
θ_{out}	[K]	64	64	64	64	64	64
T_i	[K]	29.1	37.8	44.9	51.1	56.7	62.0
Cu lead section length	[m]	0.45	0.43	0.41	0.40	0.39	0.38
HTSC lead section length	[m]	0.6	0.6	0.6	0.6	0.6	0.6
I=20 kA:							
$\dot{m}_{he}$	[g/s]	3.4	4.1	5.1	7.2	12.1	41.7
$\dot{Q}_i$ (at $T_{HTSC-Cu}$)	[W]	960	930	903	893	883	867
$\dot{Q}_{i_c}$ ($\dot{Q}_i$ equiv. at 4.5 K)	[W]	136	98	78	66	58	51
$\dot{Q}_{res_c}$ (resist. loss at 4.5 K)	[W]	0.8	0.8	0.8	0.8	0.8	0.8
$\dot{Q}_{cond_c}$ (cond. heat at 4.5 K)	[W]	0.4	0.7	0.9	1.2	1.4	1.7
$\sum \dot{Q}_c$ (loss at T_c)	[W]	138.2	99.5	79.7	68.0	60.2	53.5
I=16 kA:							
$\dot{m}_{he}$	[g/s]	2.5	3.0	3.8	5.4	9.1	31.7
$\dot{Q}_i$ (at $T_{HTSC-Cu}$)	[W]	701	687	678	671	665	657
$\dot{Q}_{i_c}$ ($\dot{Q}_i$ equiv. at 4.5 K)	[W]	99	72	59	50	44	39
$\dot{Q}_{res_c}$ (resist. loss at 4.5 K)	[W]	0.5	0.5	0.5	0.5	0.5	0.5
$\dot{Q}_{cond_c}$ (cond. heat at 4.5 K)	[W]	0.4	0.7	0.9	1.2	1.4	1.7
$\sum \dot{Q}_c$ (loss at T_c)	[W]	99.9	73.2	60.4	51.7	45.9	41.2
I=12.5 kA:							
$\dot{m}_{he}$	[g/s]	2.1	2.5	3.2	4.5	7.6	26.5
$\dot{Q}_i$ (at $T_{HTSC-Cu}$)	[W]	587	574	568	560	556	550
$\dot{Q}_{i_c}$ ($\dot{Q}_i$ equiv. at 4.5 K)	[W]	83	61	49	42	36	32
$\dot{Q}_{res_c}$ (resist. loss at 4.5 K)	[W]	0.3	0.3	0.3	0.3	0.3	0.3
$\dot{Q}_{cond_c}$ (cond. heat at 4.5 K)	[W]	0.4	0.7	0.9	1.2	1.4	1.7
$\sum \dot{Q}_c$ (loss at T_c)	[W]	83.7	62.0	50.2	43.5	37.7	34.0
I=0 kA:							
$\dot{m}_{he}$	[g/s]	1.7	2.0	2.5	3.5	5.8	19.9
$\dot{Q}_i$ (at $T_{HTSC-Cu}$)	[W]	465	452	445	432	420	414
$\dot{Q}_{i_c}$ ($\dot{Q}_i$ equiv. at 4.5 K)	[W]	66	48	39	32	28	24
$\dot{Q}_{res_c}$ (resist. loss at 4.5 K)	[W]	0.0	0.0	0.0	0.0	0.0	0.0
$\dot{Q}_{cond_c}$ (cond. heat at 4.5 K)	[W]	0.4	0.7	0.9	1.2	1.4	1.7
$\sum \dot{Q}_c$ (loss at T_c)	[W]	66.4	48.7	39.9	33.2	29.4	25.7

heat exchanger outlet temperature of 64 K, while the inlet temperature is varied from 10 to 60 K.
The current lead section between the intercept temperature level and the cold end has been simulated for Bi-2223 tapes stabilized with Ag-Au alloy. The cross section area has been fixed for a current density of $J_{Bi2223} = 17 \cdot 10^6$ A/m^2 at 16 kA and a superconductor fraction of 65 % [9]. The cross section area of the Bi-2223 superconductor is

$$A_{Bi2223} = \frac{I}{J_{Bi2223}} = \frac{16 \cdot 10^3}{17 \cdot 10^6} = 941 \cdot 10^{-6} m^2$$

and the cross section area of the Ag-Au alloy is

$$A_{Ag11\%Au} = \frac{0.35}{0.65} A_{Bi2223} = 507 \cdot 10^{-6} m^2.$$

Compared to the heat load at intercept temperature level, the resistive loss at this level is negligible. At the cold end of the current lead, the resistive loss lies in the same order than the conducted heat and has to be considered. The contact resistance between the superconducting cable and the HTSC at the current lead cold end is assumed with ≈2 nΩ [9].

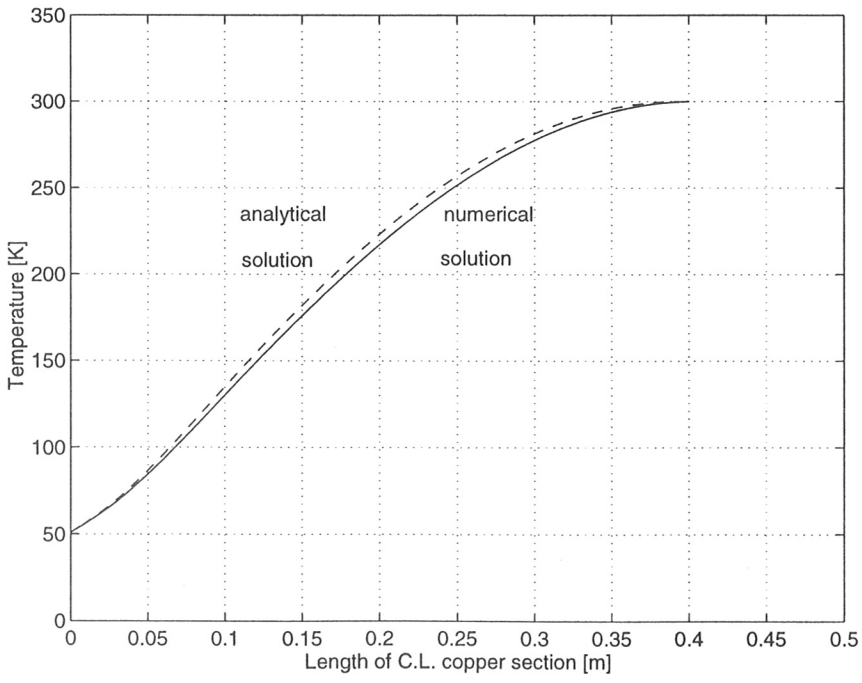

Fig. 4.1: Temperature distribution along the copper section of an optimized conduction cooled current lead (analytical and numerical solution)

Fig. 4.1 shows the temperature distributions along a conduction cooled copper lead at nominal current I_n for a helium inlet temperature of 40 K. The values are deduced from analytical and numerical model, respectively (see chapters 2 and 3). Both characteristics are in good

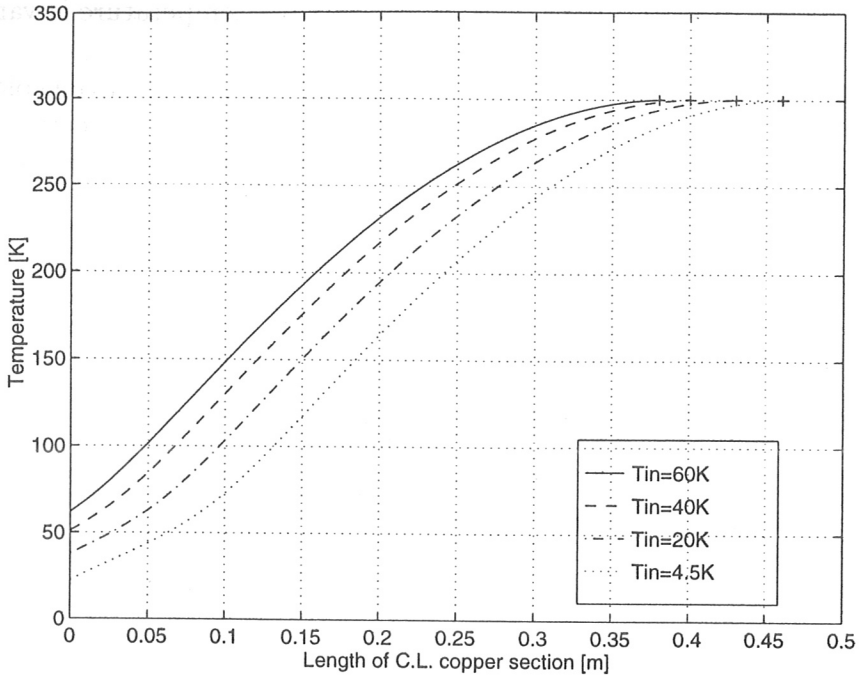

Fig. 4.2: Temperature distribution along the copper section of optimized conduction cooled current leads (Heat exchanger inlet temperature: 4.5 K, 20 K, 40 K, and 60 K)

agreement. The differences between both solutions appear due to linearization of the analytical model by applying the Wiedemann-Franz law.
In case of optimizing the relation between copper cross section and copper lead length to fulfil the Neumann condition, the length decreases with increasing helium inlet temperature (Fig. 4.2).
Fig. 4.3 shows the temperature distribution for currents in the range $0 \leq I_n \leq 1.25 I_n$. At current greater than the nominal value I_n, the temperature gradient dT/dx at the hot end becomes negative and the lead may overheat. The supercondutor fraction in the tape is assumed with 0.65 for a current density of $17 \cdot 10^6$ A/m^2.
The heat leak at intercept temperature level is a function of electrical current and intercept temperature. In order to get a common base to compare the heat leaks for different intercept temperatures, the equivalent value is determined at 4.5 K. (Fig. 4.4).
Increasing the helium inlet temperature level at fixed helium outlet temperature requires a higher helium mass flow rate in order to absorb the loss at intercept temperature (Fig. 4.5).
The heat leak at the current lead cold end becomes higher by increasing the intercept temperature level (Fig. 4.6). Responsible for this effect is mainly the heat conductivity of the alloy, as shown in Fig. 1.5. It is more than one order of magnitude higher than that of the superconducting material.

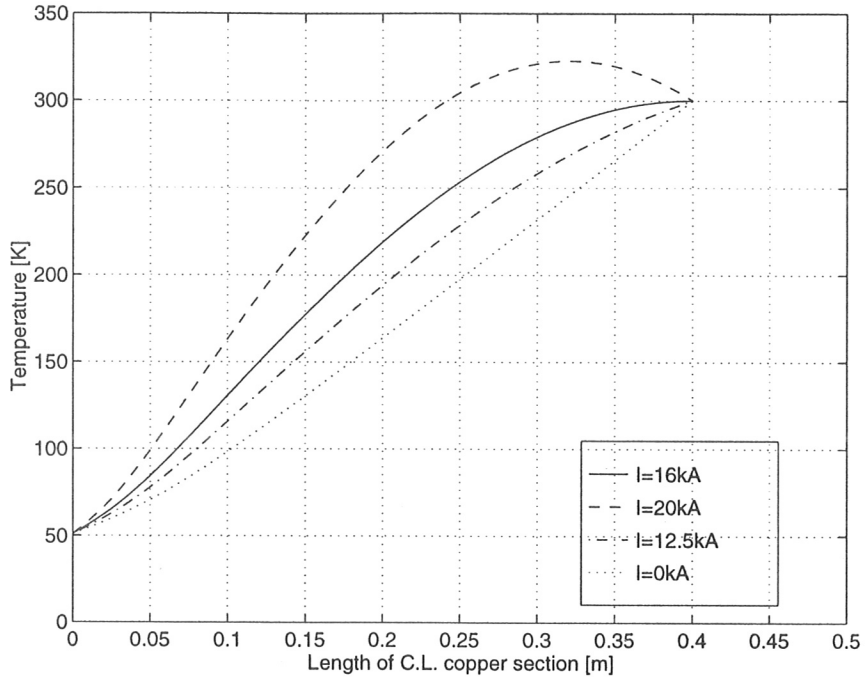

Fig. 4.3: Temperature distribution along the copper section of an optimized conduction cooled current lead at 0 kA, 12.5 kA, 16 kA, and 20 kA (Intercept temperature: 50 K)

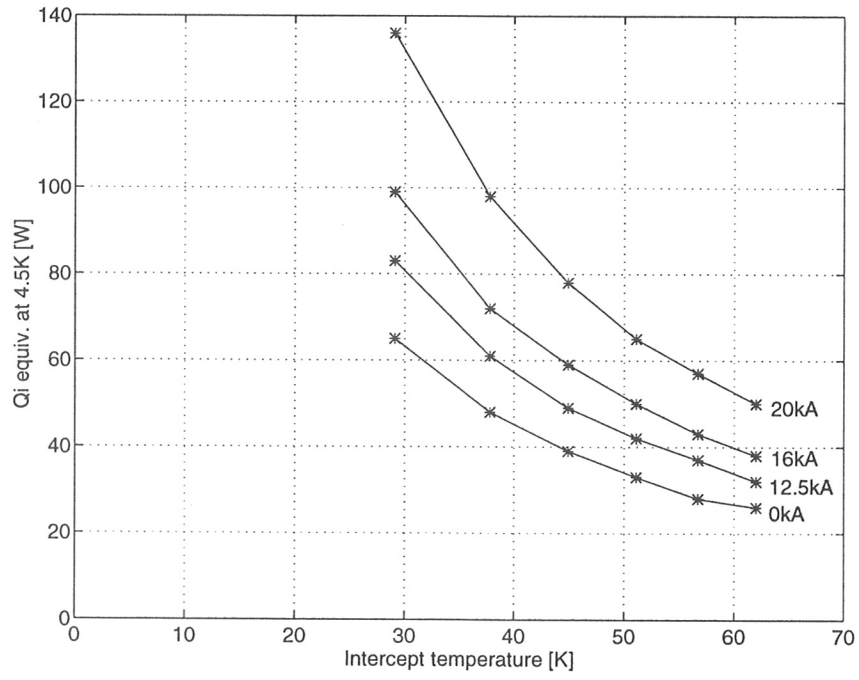

Fig. 4.4: Heat leak $\dot{Q}_i$ equivalent at 4.5 K for different intercept temperature values (Current: 0 kA, 12.5 kA, 16 kA, and 20 kA)

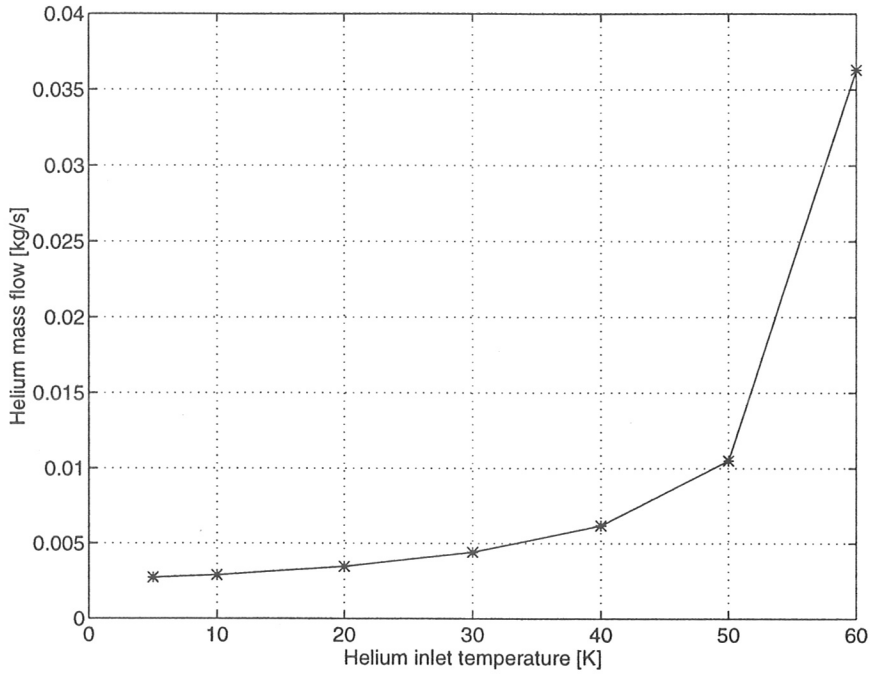

Fig. 4.5: Helium mass flow rate through the heat exchanger versus intercept temperature

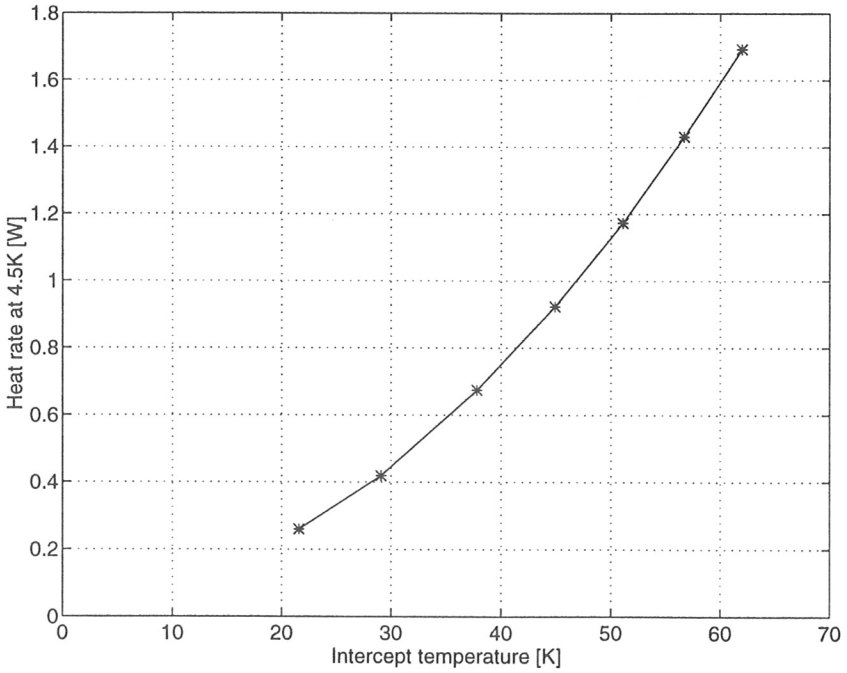

Fig. 4.6: Heat leak due to thermal conduction along the HTSC tape versus intercept temperature

4.2 Forced-flow cooled current leads

This section describes the solutions for forced-flow cooled 16 kA current leads. Calculations have been performed with parameters as given in Table 4.2.

Table 4.2: Input parameters for forced-flow cooled current leads

Nominal current	[A]	16000	
Current density	[Am^{-2}]	10^7	[22]
Copper cross section	[m^2]	$16 \cdot 10^{-3}$	
RRR	[-]	30	
Contact resistance at T_i	[nΩ]	$\approx$15	[9]
Contact resistance at T_c	[nΩ]	$\approx$2	[9]
Helium pressure	[Pa]	$4 \cdot 10^5$	
p · h	[W/(m K)]	5000	[22]
rel. refrigerator efficiency	[%]	25	[7]

In forced-flow cooled current leads, a temperature difference between the lead and the coolant of $(T - \theta) \leq 2$ K seems a good approximation in order to determine the heat leak at the cold end of the copper part above the interconnection to the HTSC [22].
The input power to a given refrigerator is a function of a number of criteria. The most important of which is the amount of refrigeration being produced by the refrigeration plant [7]. The refrigeration input power can be stated as

$$\dot{Q}_{rip} = \frac{\dot{Q}_{cip}}{\eta}, \tag{4.4}$$

where $\dot{Q}_{cip}$ is the carnot input power for helium gas recooling and η is the relative refrigerator efficiency. For the W7-X refrigerator $\eta \approx 0.25$ can be assumed. The carnot input power for recooling of forced-flow cooled current leads is

$$\dot{Q}_{cip} = \dot{m} \left[T_h \left(s_h - s_c\right) - \left(h_h - h_c\right)\right]. \tag{4.5}$$

The heat flux at intercept temperature $\dot{Q}_i$ referred to the hot end temperature T_h gives

$$\dot{Q}_{i_h} = \dot{Q}_i \frac{T_h - T_i}{T_i}. \tag{4.6}$$

The refrigeration power, to be minimized for an optimized operation of the current leads, is

$$\dot{Q}_{ref} = \dot{Q}_{cip} + \dot{Q}_{i_h}. \tag{4.7}$$

The loss due to contact resistance is calculated by

$$\dot{Q}_{res} = I^2 R \tag{4.8}$$

with I the current and R the contact resistance at intercept level and current lead cold end, respectively.

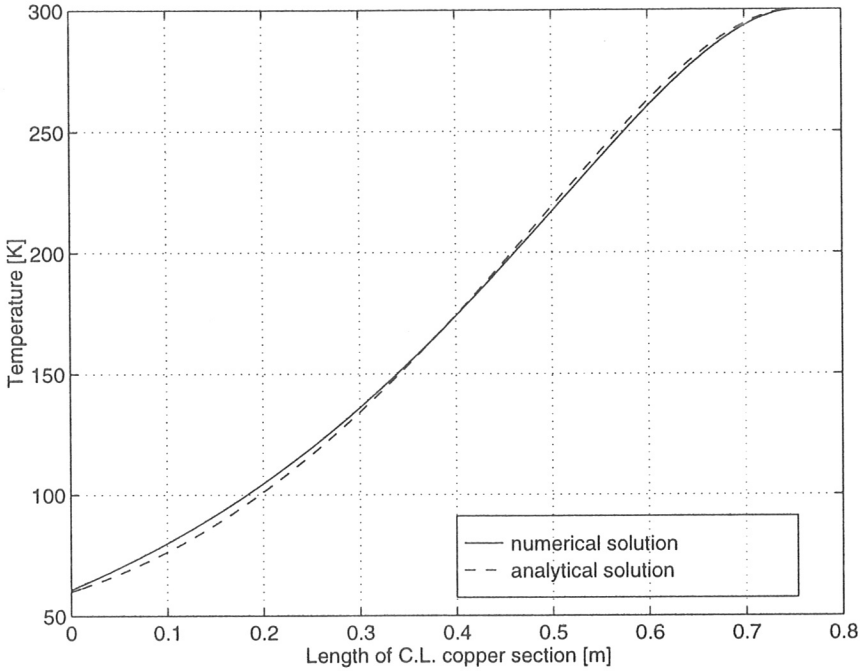

Fig. 4.7: Temperature distribution along the copper section of an optimized forced-flow cooled current lead at nominal current (analytical and numerical solution)

Fig. 4.7 compares the solution of analytical and numerical simulation of the temperature distribution along the copper current lead section. Differences in the results are mainly determined by the influence of heat exchange between copper and helium.

Forced-flow cooled current leads can be optimized by applying the Neumann condition $dT/dx = 0$ at the current lead hot end by varying the length and the coolant mass flow rate. Therefore, the required helium mass flow rate is calculated for a given length of the copper section. The shorter the current lead section, the smaller becomes the helium mass flow rate. On the other hand, the conducted heat from the current lead hot end rises with decreasing length. Carnot input power and loss are listed in Table 4.3.
Fig. 4.8 shows the carnot input power for recooling the forced-flow cooled current leads with helium by minimizing the heat leak at intercept temperature ($dT/dx = 0$ at $T = T_h$).

Table 4.3: Results for a single forced-flow cooled binary current lead at $I = 16$ kA and $T_i = 60$ K by varying the length of the copper section

Copper section:								
Length	[m]	0.50	0.60	0.70	0.80	0.90	1.00	1.10
L/A	[m^{-1}]	312.5	375.0	437.5	500.0	562.5	625.0	687.5
$\dot{m}_{he}$	[g/s]	0.45	0.62	0.82	0.92	1.00	1.08	1.15
Carnot input power:								
$\dot{Q}_{cip}$ (CIP for recooling)	[W]	571	780	1030	1159	1262	1361	1452
Heat load at intercept temperature:								
$\dot{Q}_{\lambda_i}$ (heat flux at T_i)	[W]	514	342	219	154	117	93	77
$\dot{Q}_{res_i}$ (resist. loss at T_i)	[W]	4	4	4	4	4	4	4
$\sum \dot{Q}_i$ (loss at T_i equiv. at 300 K)	[W]	2070	1382	893	629	483	385	322
Superconductor section:								
Length	[m]	0.60	0.60	0.60	0.60	0.60	0.60	0.60
Heat loads at cold end:								
$\dot{Q}_{\lambda_c}$ (heat flux at T_c))	[W]	1.6	1.6	1.6	1.6	1.6	1.6	1.6
$\dot{Q}_{res_c}$ (resist. loss at 4.5 K)	[W]	0.5	0.5	0.5	0.5	0.5	0.5	0.5
$\sum \dot{Q}_c$ (loss at T_c equiv. at 300 K)	[W]	138	138	138	138	138	138	138
$\dot{Q}_{ref}$ (refrig. power at 300 K)	[W]	2779	2300	2061	1926	1883	1884	1912

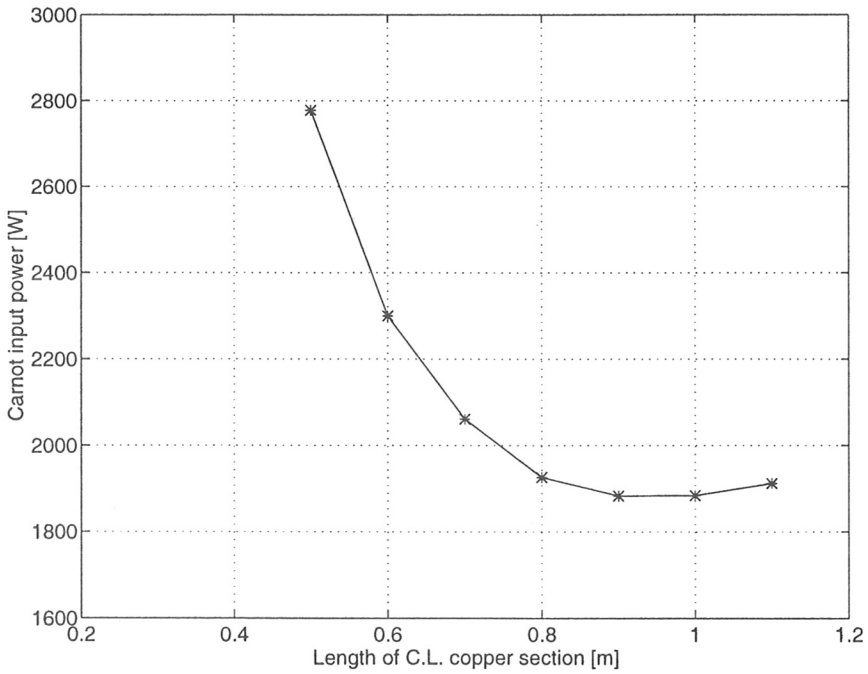

Fig. 4.8: Carnot input power for versus current lead length for $dT/dx = 0$ at the current lead hot end

The intercept temperature level of a forced-flow cooled current lead (Fig. 1.1c) is margined by the cold end temperature of the current lead and the critical temperature of the HTSC. In order to determine the helium mass flow rate dependence on the intercept temperature level, the solutions in Fig. 4.9 consider a fixed length of the copper section. The helium mass flow rate grows with increasing intercept temperature level (Fig. 4.10) while the required refrigeration power at room temperature decreases. From the point of refrigeration power, the intercept temperature should be as high as possible. Table 4.4 lists the carnot input power and loss for current lead operation at different intercept temperature levels. The first column shows the data for a 1 m long conventional copper lead without HTSC part [7].

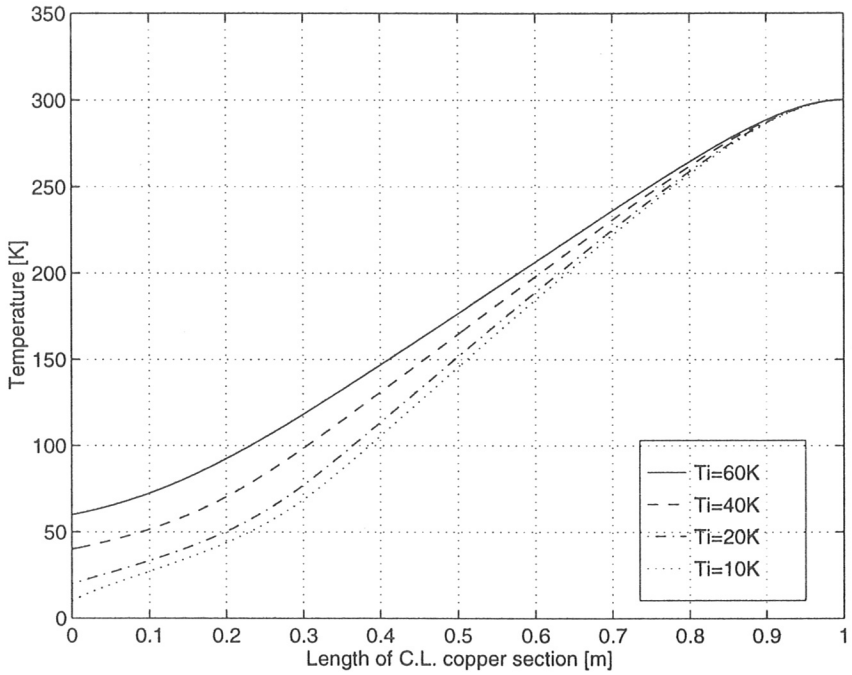

Fig. 4.9: Temperature distribution along a forced-flow cooled current lead at nominal current (Intercept temperature: 10 K, 20 K, 40 K, and 60 K)

The stellarator W7-X will be operated at different current levels. The required helium mass flow rate depends on the current level. Fig. 4.11 shows the helium mass flow rate dependency on current levels between $0 \leq I_n \leq 1.25\, I_n$. Carnot input power and loss for current lead operation at different supply current levels are listed in Table 4.5.

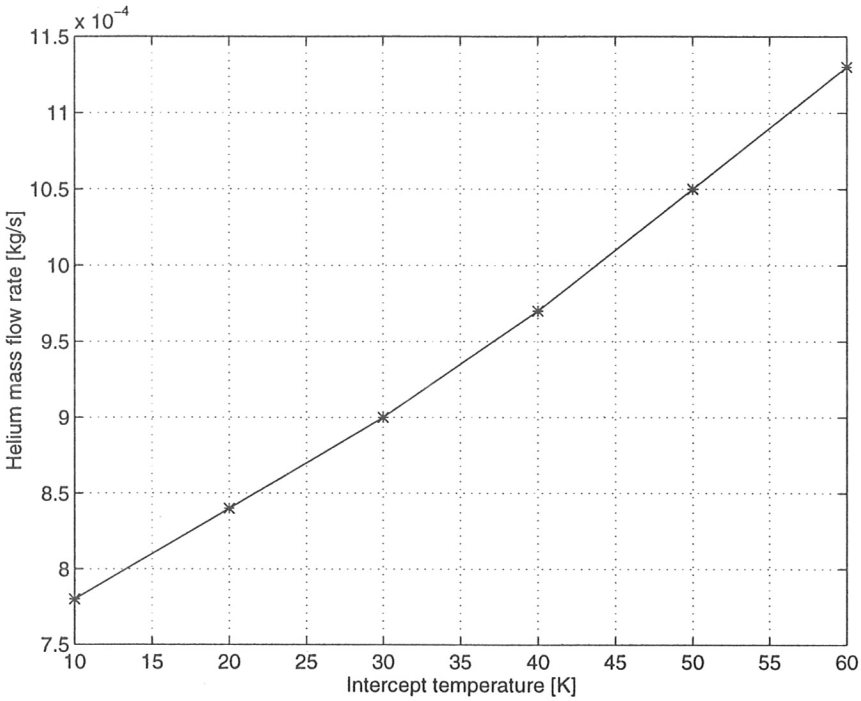

Fig. 4.10: Helium mass flow rate versus intercept temperature in the forced-flow cooled copper section at nominal current

Table 4.4: Results for a single forced-flow cooled binary current lead at $I = 16$ kA and $l = 1$ m by varying the intercept temperature

Intercept temperature:	[K]	4.5	10	20	30	40	50	60
Carnot input power:								
$\dot{m}_{he}$	[g/s]	0.72	0.78	0.84	0.90	0.97	1.05	1.15
$\dot{Q}_{ci}$ (Carnot input power)	[W]	3605	2958	2323	1967	1735	1568	1450
Loads at 4.5 K:								
$\dot{Q}_{ci4.5K}$ (equiv. CIP at 4.5 K)	[W]	54.9	45.1	35.4	29.9	26.4	23.9	22.1
$\dot{Q}_{res_c}$ (resist. loss at 4.5 K)	[W]	0.8	0.8	0.8	0.8	0.8	0.8	0.8
$\dot{Q}_{cond_c}$ (cond. heat at 4.5 K)	[W]	43.0	2.0	1.9	1.7	1.4	1.2	0.9
$\sum \dot{Q}_c$ (loss at T_c)	[W]	98.7	47.9	38.1	32.4	28.6	25.9	23.8
Room temperature:								
$\dot{Q}_{rt}$ (refrig. power $\eta_c = 0.2$)	[kW]	32.4	15.7	12.5	10.6	9.4	8.5	7.8

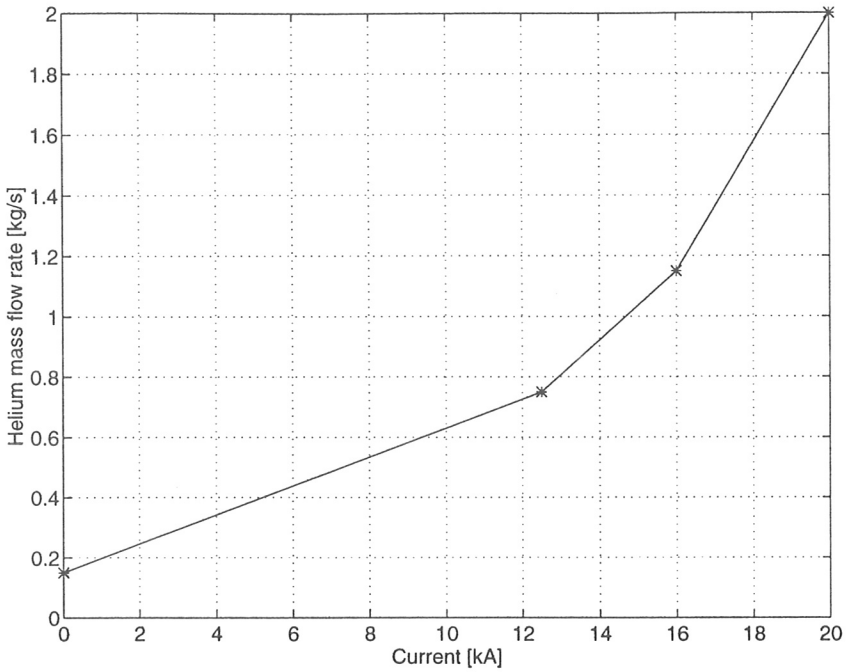

Fig. 4.11: Helium mass flow rate versus current in the forced-flow cooled copper section

Table 4.5: Results for a single forced-flow cooled binary current lead at $T_i = 60$ K and $l = 1$ m by varying the current

Current	[kA]	0	12.5	16	20
Carnot input power:					
$\dot{m}_{he}$	[g/s]	0.15	0.75	1.15	2.0
$\dot{Q}_{ci}$ (Carnot input power)	[W]	189	946	1450	2522
Loads at 4.5 K:					
$\dot{Q}_{ci4.5K}$ (equiv. CIP at 4.5 K)	[W]	2.9	14.4	22.1	38.4
$\dot{Q}_{res_c}$ (resist. loss at 4.5 K)	[W]	0.0	0.4	0.8	1.0
$\dot{Q}_{cond_c}$ (cond. heat at 4.5 K)	[W]	2.2	2.0	0.9	0.7
$\sum \dot{Q}_c$ (loss at T_c)	[W]	5.1	16.8	23.9	40.1
Room temperature:					
$\dot{Q}_{rt}$ (refrig. power $\eta_c = 0.2$)	[kW]	1.7	5.5	7.9	13.2

Chapter 5

Conclusions

For the preliminary assumed materials and concepts, use of high temperature superconductors reduce the heat leak at the current lead cold end by a factor of 4, compared to a conventional gas-cooled copper current lead.
The equivalent loss at 4.5 K for conduction cooled current leads is larger than for forced-flow cooled current leads. But, conduction cooled current leads just require helium gas cooling from heat exchanger outlet temperature (< 70 K) down to it's inlet temperature level. In forced-flow cooled current leads, refrigeration is necessary from room temperature down to intercept temperature level.
The cooling concept depends mainly on the refrigeration environment. The higher the intercept temperature level, the lower will be the required refrigeration power. From the point of current lead, the intercept temperature should be below 60 K. Above this temperature, the current density of the HTSC decreases dramatically.

Most of the simulations have been performed for a current lead length of 1 m. The real length for the W7-X will be determined later. Accurate calculations have to be performed dependent on proper current lead design and materials, and the specified refrigeration plant.

Acknowledgment

I would like to express my gratitude to Felix Schauer, leader of the cryogenic group, for his advises and fruitful discussions. His expert opinion has been valuable and encouraging for the development of this study.

Bibliography

[1] A. Ballarino, A. Ijspeert, M. Teng, U. Wagner, S. Harrison, K. Smith, and L. Cowey, *Design of 12.5 kA current leads for the Large Hadron Collider using high temperature superconductor material*, Lhc project report 62, CERN LHC Division, CH-1211 Geneva 23, October 1996.

[2] Yu. L. Buyanov, *Current leads for use in cryogenic devices. principle of design and formulae for design calculations*, Cryogenics **25** (1985), 94–110.

[3] Cryodata Inc., Florence, SC 29501, *User's guide to CRYOCOMP*, 2.0 ed., January 1995.

[4] G. Friesinger, R. Heller, W. Herz, M. Irmisch, G. Nöther, L. Schappals, K. Schweikert, L. Siewerdt, M. Süsser, A. Ulbricht, F. Wüchner, and G. Zahn, *Test der zwangsgekühlten 30 kA/23 kV Stromzuführung in der Toska-Anlage -Teil 1-*, Tech. Report KfK Primärbericht 31.03.05P02A, Kernforschungszentrum Karlsruhe, Karlsruhe, December 1992.

[5] ———, *Test der zwangsgekühlten 30 kA/23 kV Stromzuführung in der Toska-Anlage -Teil 2-*, Tech. Report KfK Primärbericht 31.03.05P04A, Kernforschungszentrum Karlsruhe, Karlsruhe, June 1993.

[6] H. Fujishiro, M. Ikebe, K. Noto, and M. Matsukawa, *Low thermal conductive Bi-2223 tapes sheated with Ag-Au alloys*, IEEE Transactions on Magnetics **30** (1994), no. 4, 1645–1650.

[7] M. A. Green, *The effect of superconductor on gas cooled leads for superconducting magnets*, LBL internal report lbid-1591, Lawrence Berkeley Laboratory, Berkeley, CA, April 1990.

[8] R. Heller, *Assessment of the use of high temperature superconductors in the ITER current leads*, Tech. Report NET 94-358, Forschungszentrum Karlsruhe, Karlsruhe, July 1995, final report.

[9] R. Heller, G. Friesinger, W. Herz, M. Irmisch, G. Nöther, L. Schappals, K. Schweikert, L. Siewerdt, M. Süsser, A. Ulbricht, F. Wüchner, and G. Zahn, *Test of a forced-flow cooled 30 kA/23 kV current lead for the POLO model coil*, IEEE Transactions on Magnetics **30** (1994), no. 4, 2387–2390.

[10] R. Heller and J. R. Hull, *Conceptual design of a forced-flow-cooled 20 kA current lead using Ag-alloy-sheathed Bi-2223 high-temperature superconductors*, Tech. Report KfK 5172, ANL-94/36, Kernforschungszentrum Karlsruhe, Karlsruhe, November 1994.

[11] M. K. Jain, *Numerical solution of differential equations*, Second ed., Wiley Eastern Limited, India, 1984.

[12] G. Krainz, *Quench protection and powering in a string of superconducting magnets for the Large Hadron Collider*, Ph.D. thesis, University of Technology Graz and CERN Geneva, 1997.

[13] M. Matsukawa, K. Iwasaki, T. Sasaki, N. Koboyashi, K. Yoshida, K. Zikihara, and M. Ishihara, *Thermal conductivity of the c-axis aligned* $(Bi,Pb)_2Sr_2Ca_2Cu_2O_y$ *in the superconducting and mixed states*, Cryogenics **37** (1997), 255–262.

[14] M. S. McAshan, *MIITS integrals for copper and for Nb-46.5 wt% Ti*, SSC Note SSC-N-468, SSC Central Design Group, Berkeley, CA, February 1988.

[15] W. Mercouroff, *Minimization of thermal losses due to electrical connections in cryostats*, Cryogenics **3** (1963), 171–173.

[16] K. Nomura, T. Sasaoka, J. Sato, S. Kuma, H. Kumakura, K. Togano, and N. Tomita, *Influence of Ag-Au and Ag-Cu alloys on* $Bi_2Sr_2CaCu_2O_x$ *superconductor*, Appl. Phys. Lett. **64** (1994), 112–114.

[17] F. Ramsauer, *Strom- und Kühlmittelzuführung für Rotoren von supraleitend erregten Synchrongeneratoren*, Ph.D. thesis, University of Technology, Graz, 1991.

[18] F. Schauer, *Cooling system for Wendelstein 7-X*, Symposium on Cryogenic Systems for Large Scale Superconducting Applications (Toki, Japan), NIFS, May 1996.

[19] ———, *Kälteversorgungssystem des Kernfusionsexperimentes Wendelstein 7-x*, (Hamburg), Deutsche Kälte-und-Klimatagung 1997, November 1997.

[20] S. W. Van Sciver, *Helium Cryogenics*, Plenum Press, New York, 1986.

[21] M. Teng, A. Ballarino, R. Herzog, A. Ijspeert, C. Timlin, S. Harrison, and K. Smith, *Evaluation of HTS samples for 12.5 kA current leads*, Eucas report, CERN LHC Division, 1997.

[22] R. Wesche and A. M. Fuchs, *Design of superconducting current leads*, Cryogenics **34** (1994), 145–154.

[23] M. N. Wilson, *Superconducting magnets*, Clarendon Press, Oxford, 1983.

[24] S. Yang and J. M. Pfotenhauer, *Optimization of the intercept temperature for high temperature superconducting current leads*, Advances in Cryogenic Engineering **41** (1996), 567–572.